

Structural transition at the subsurface of few-layer Bi(110) film during the growth

Tetsuroh Shirasawa^{1,*}, Wolfgang Voegeli², Etsuo Arakawa², Ryota Ushioda³, Kan Nakatsuji⁴, and Hiroyuki Hirayama³

¹*National Metrology Institute of Japan (NMIJ), National Institute of Advanced Industrial Science and Technology (AIST), 1-1-1 Higashi, Tsukuba, Ibaraki 305-8565, Japan*

²*Department of Physics, Tokyo Gakugei University, 4-1-1 Nukuikita-machi, Koganei, Tokyo 184-8501, Japan*

³*Department of Physics, Tokyo Institute of Technology, J1-3 4259 Nagatsuda, Midori-ku Yokohama 226-8502, Japan*

⁴*Department of Materials Science and Engineering, Tokyo Institute of Technology, J1-3 4259 Nagatsuda, Midori-ku Yokohama 226-8502, Japan*



(Received 20 October 2022; accepted 27 February 2023; published 24 March 2023)

The structure and growth behavior of Bi(110) ultrathin films on Si(111)-7 × 7 substrate are studied using real-time x-ray crystal truncation rod scattering measurements. The film grows in units of bilayers up to four atomic layers and shows a quasi-layer-by-layer growth above four layers in which even-layer-height domains are preferentially formed. It is revealed that the even-layer-height domains fully consist of black-phosphorus-like paired layers while the odd-layer-height domains have an additional bulk-Bi(110)-like layer beneath the top bilayer. This suggests that a structure change occurs at the subsurface when an additional single layer grows on the even or odd domains. Monte Carlo simulations indicate that a smaller free energy of the even structure than the odd structure leads to the preferential formation and that a small interface energy at the even/odd domain boundary allows the frequent transitions during the growth.

DOI: [10.1103/PhysRevMaterials.7.033404](https://doi.org/10.1103/PhysRevMaterials.7.033404)

I. INTRODUCTION

Few-layer pnictogens with a black phosphorus (BP) structure or BP-analog binary and ternary materials have attracted considerable attention in a broad range of research fields [1–7], because of their unique properties such as prominent carrier mobility [8], anisotropic photon absorption [9], high capacity for metal ion storage [10], and high catalytic activity [11]. In particular, heavy pnictogens (Bi and Sb) with a BP-like structure are of great interest as they are predicted to host novel two-dimensional Dirac and Weyl states [12–17].

Few-layer-thick Bi ultrathin films adopt the [110] growth orientation (rhombohedral notation) on various substrates regardless of lateral lattice mismatch [18–30]. The Bi films show a complex growth behavior, including the formation of wetting layers, preferential film thicknesses [28], and a transformation to the [111] orientation at a critical film thickness [18,31]. For the structure of Bi(110) films, three different models have been proposed [Figs. 1(a)–1(c)]: a bulk Bi(110) structure in which each monolayer (ML) forms covalent bonds with the adjacent MLs, a BP-like structure, which consists of paired MLs with a vertical buckling in each ML, and a sandwich structure, which contains bulk-Bi(110)-like layers sandwiched by top and bottom BP-like bilayers (BLs) [12,28,32]. The structure has been studied mainly using scanning tunneling microscopy (STM). On most substrates even-layer-height domains (hereafter, even domains) and less-populated odd-layer-height domains (odd domains) were observed. The structure of the even domains was ascribed to the BP-like structure [28] or the sandwich structure [22]. For the odd domains the sandwich structure

was suggested, based on the surface lattice alignment between the even and odd domains [28]. However, the structures of internal layers, such as stacking structure, interlayer distance, and vertical buckling remain to be clarified. The structure determination is necessary for understanding the nature of the few-layer Bi(110) films, as the electronic structures depend on the stacking structures [33,34] and the topological properties can be varied by either in-plane or out-of-plane strains [13,35], amplitude of the vertical buckling [12,36], interlayer distances [36], and film thickness [32,37].

In this paper, we report the structure and growth behavior of few-layer Bi(110) ultrathin films grown on a Si(111)-7 × 7 substrate, studied by real-time x-ray crystal truncation rod (CTR) measurements [38–41], which allow the structure and coverage of each ML to be quantified during the growth [Fig. 1(e)]. The change in coverage of each ML shows that the film grows in units of BL up to four MLs and changes to a quasi-layer-by-layer growth above four MLs with a preferential population of the even domains. The structure analysis clarifies that the even domains fully consist of BP-like BLs and suggests a new structure model for the odd domains, which has an additional bulk-Bi(110)-like ML located beneath the top BL [Fig. 1(d)]. The growth behavior is reproduced by Monte Carlo (MC) simulations that include the free energy change due to the structure transition between the even and odd structures, suggesting that a smaller free energy of the even structure than the odd structure leads to the preferential even domain formation.

II. RESULTS AND DISCUSSION

A. Structure of 4-ML-thick Bi(110) film

All the experiments were conducted in an ultrahigh vacuum (10^{-8} Pa). Details of the experiments and analysis are

*t.shirasawa@aist.go.jp

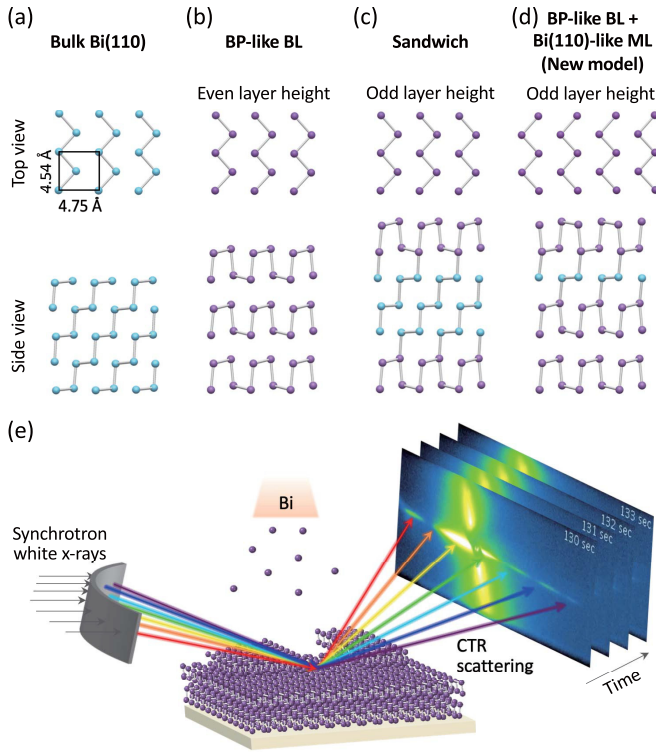


FIG. 1. (a)–(d) Top and side views of the structure models of few-layer Bi(110) films. The in-plane unit cell is indicated in (a). The top views show only the surface ML. (e) A schematic illustration of real-time x-ray CTR scattering measurements with a wavelength-dispersive mode [38–41] during the growth of Bi(110) film.

described in the Supplemental Material [42]. First, the out-of-plane structure of nearly 4-ML-thick Bi(110) was analyzed by static CTR measurements. The specular CTR ($00L$ rod) profile was measured, and the interlayer distance, buckling amplitude, and coverage (1 ML is defined as the density of Bi atoms in the bulk Bi(110) ML, 9.27×10^{14} atoms/cm²) of each ML were deduced by fitting the CTR profile with a least-squares method. Since the Bi(110) domains have a random in-plane orientation and show weak diffraction rings [18], which were difficult to measure accurately, the in-plane atomic structures could not be analyzed. As shown in Fig. 2(a), the CTR profile

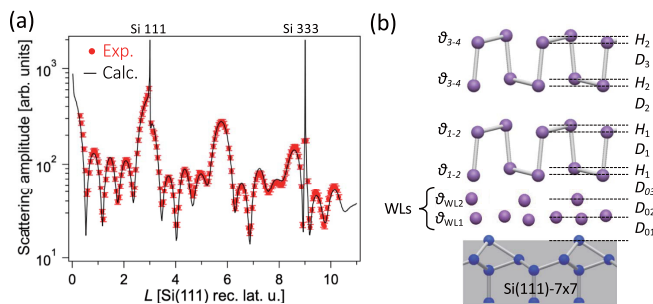


FIG. 2. (a) Measured (symbols) and calculated (solid curve) $00L$ CTR scattering profiles of the nearly 4-ML-thick Bi(110) film grown on the Si(111)- 7×7 substrate. (b) Structure model of the film. Interlayer distances D , amplitudes of vertical buckling H , and layer coverages θ optimized in the structure analysis are indicated.

shows Laue oscillations from the Bi layers and is nicely reproduced by the profile calculated for the BP-like structure. The R -factor value, a measure of the agreement, is 0.06. The structure model consists of aperiodic wetting layers (WLs) and the BP-like BLs grown on the WLs, as shown in Fig. 2(b). The fitting parameters are shown in Fig. 2(b) and the optimal values are shown in Table I. We also optimized an isotropic Debye-Waller factor, which represents the thermal vibration and a possible structural inhomogeneity. The optimized amplitudes are 0.19 ± 0.05 Å for the WLs and 0.14 ± 0.05 Å for the Bi(110) layers, respectively. The optimized structure is almost the same as the BP-like BLs grown on a Si(111)- $\sqrt{3} \times \sqrt{3}$ -B substrate [43]. We note that the film contained small amounts of fifth (0.13 ± 0.02 ML) and sixth MLs (0.1 ± 0.02 ML) with the structures described below.

The determined structure is consistent with the previous STM and theoretical studies. The buckling amplitude in the top ML ($H_2 = 0.39 \pm 0.03$ Å) is consistent with the STM studies on different substrates (0.32 Å [20] and 0.31 Å [27]). The thickness of the top BL ($D_2 + D_3 + 2H_2 = 6.42 \pm 0.07$ Å) is consistent with the STM studies, around 6.6 Å [18,28,36]. The height difference between the buckled-up (or -down) atoms in the bottom and top BLs ($H_1 + D_1$ and $H_2 + D_3$), which would be close to the interlayer covalent bond lengths within the BLs, are 3.2 ± 0.06 Å and 3.09 ± 0.05 Å, respectively. These values are close to the bond length of 3.10 Å obtained by the first-principles calculations [32]. Here, we discuss the stacking structure of BP-like BLs, based on the interlayer distances. The previous STM study for the Bi(110) films on Cu(111) suggested AA stacking, which has the buckled-up on -up and buckled-down on -down configuration at the BL-BL junction as shown in Fig. 2(b), based on scanning tunneling spectroscopy measurements [36]. The present result supports the AA stacking, as the height difference between the buckled-down atoms ($D_2 + H_1 = 3.27 \pm 0.07$ Å) and buckled-up atoms ($D_2 + H_2 = 3.33 \pm 0.05$ Å) are almost identical to the values obtained by the first-principles calculations for the AA stacking, 3.33 Å [36] and 3.4 Å [32]. We note that a buckled-up on -down BL-BL junction (e.g., the AC stacking [36]) is unlikely, because the interlayer distance of $D_2 = 2.94 \pm 0.04$ Å is significantly smaller than the covalent bond length in bulk Bi crystal, 3.064 Å.

B. Structure transition of Bi(110) film during the growth

The structure and growth behavior of thicker films were studied by real-time CTR measurements. $00L$ CTR profiles were measured with a temporal resolution of 1 s during the growth (the Bi deposition rate was 0.032 ML/s). Some of the CTR profiles are shown in Fig. 3(a), and all the detector images and CTR profiles are shown in the Supplemental Material [44]. For most of the CTR data the uncertainty in the measured value is in the range of 5–10%. Around the Bragg peaks of Bi(110) and Si(111), their thermal diffuse scatterings (TDSs) spread over the neighboring detector pixels so that a suitable background subtraction was difficult. Therefore, we excluded the data around the Bragg peaks. The CTR profiles show Laue oscillations from the Bi(110) layers, and the period of the Laue oscillations decreases with

TABLE I. Optimized values of the fitting parameters of the nearly 4-ML-thick Bi(110) film, obtained from the static CTR scattering measurements (see Fig. 2).

Interlayer distance D [Å]						Buckling H [Å]		Coverage θ [ML]			
D_{01}	D_{02}	D_{03}	D_1	D_2	D_3	H_1	H_2	θ_{WL1}	θ_{WL2}	θ_{1-2}	θ_{3-4}
$1.39_{\pm 0.03}$	$1.02_{\pm 0.03}$	$2.25_{\pm 0.04}$	$2.87_{\pm 0.04}$	$2.94_{\pm 0.04}$	$2.70_{\pm 0.03}$	$0.33_{\pm 0.06}$	$0.39_{\pm 0.03}$	$1.08_{\pm 0.08}$	$0.15_{\pm 0.03}$	$0.88_{\pm 0.07}$	$0.88_{\pm 0.07}$

increasing deposition time, showing the growth of Bi(110) layers. The CTR profiles were fitted with the least-squares method, and the interlayer distance, buckling amplitude, and coverage of each ML were obtained at each time step. Note that a diffraction peak of Bi(111) domains appeared above 200 s as indicated in Fig. 3(a), due to the phase transition from Bi(110) to Bi(111) layers [18,31,45]. We estimated the fraction of the Bi(111) domain in the analysis, assuming the Bi(111) structure obtained by the previous CTR study [45], and found that the Bi(111) domains appeared at around 200 s and gradually increased to 10% of the total area at 560 s. In this paper, we focus on the structure and growth behavior of the Bi(110) layers and do not discuss the Bi(110) \rightarrow (111) phase transition, assuming that the Bi(111) domains did not affect the growth of Bi(110) domains significantly.

All the CTR profiles were successfully reproduced by the calculations as shown in Fig. 3(a) and the Supplemental Material [44]; the R -factor values are in the range from 0.05–0.11. The resulting structures and layer coverages are

summarized in Figs. 3(b) and S2(b) [42], respectively. As seen in Fig. S2(b), the film grew in units of BL up to four MLs and the odd domains appeared above four MLs, in agreement with the previous STM studies [28,36,46]. In the analysis, we assumed that both of the even and odd domains had the BP-like BLs at the top and bottom considering that the BP-like BL eliminates the surface dangling bonds [18], and the structures of the BLs and WLs were fixed to those obtained for the nearly 4-ML-thick film (Fig. 2 and Table I). In the analysis of internal layers, first, we tried to optimize individual periodic structures for the even and odd domains, assuming the BP-like and sandwich structures, respectively, and found that they converged to an identical structure within error except for the residual ML in the odd domains. Therefore, in the final optimization, we assumed the identical structure for the common layers as shown in Fig. 3(c).

Figure 3(b) shows the interlayer distances and buckling amplitudes of the internal layers of the Bi(110) film thicker than four MLs. The values do not change significantly over the

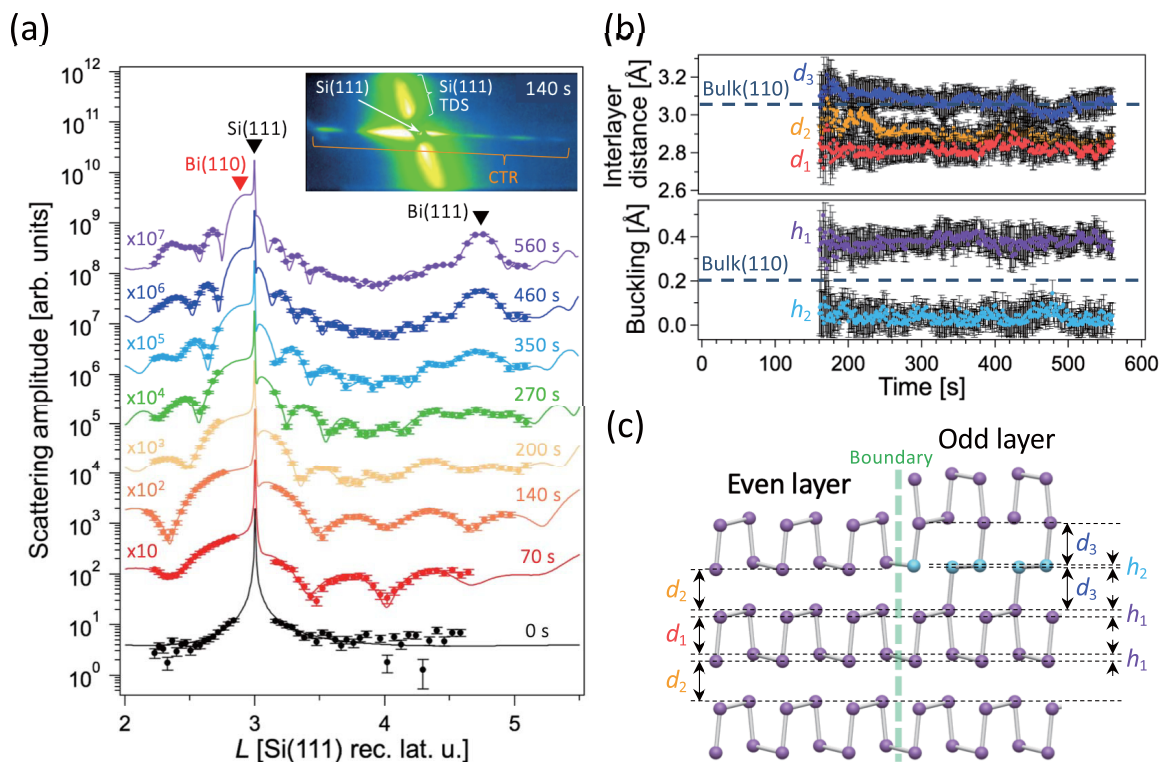


FIG. 3. (a) Measured (symbols) and calculated (solid curves) 00L CTR scattering profiles of the growing Bi(110) film. Bragg peaks of the Bi(110) domain, Bi(111) domain, and Si(111) substrate are indicated. The inset is a detector image at 140 s, in which the CTR scattering, Si(111) Bragg peak (attenuated by a beam stop), and a thermal diffuse scattering (TDS) from Si(111) are indicated. (b) Interlayer distances (top panel) and buckling amplitudes (bottom panel) of the internal layers of the Bi(110) film thicker than four MLs, obtained from the real-time CTR scattering data. Dashed lines indicate the corresponding values of bulk Bi crystal. (c) Structure model of the even and odd structures. The interlayer distances d and buckling amplitudes h are indicated. Dashed vertical line indicates an even/odd domain boundary.

deposition time, indicating no significant structure relaxations during the growth. The time-averaged values are $d_1 = 2.82 \pm 0.07 \text{ \AA}$, $d_2 = 2.90 \pm 0.07 \text{ \AA}$, and $h_1 = 0.38 \pm 0.07 \text{ \AA}$. They are different from the corresponding values of bulk Bi crystal, 3.064 \AA and 0.2 \AA , and thus reject the sandwich structure. For another model, termed Brick phase [24,47], its buckling amplitude is negligible and inconsistent with the value of h_1 . Therefore, the Brick phase is unlikely in the present system. In contrast, the values are consistent with BP-like BLs (see Fig. 2 and Table I): the value of d_1 is between the values of the bottom ($2.87 \pm 0.04 \text{ \AA}$) and top ($2.70 \pm 0.03 \text{ \AA}$) BLs of the nearly 4-ML-thick Bi(110) film and the values of d_2 and h_1 are identical to those of the BLs ($2.94 \pm 0.04 \text{ \AA}$ and $0.33 \pm 0.06 \text{ \AA}$ or $0.39 \pm 0.03 \text{ \AA}$) within the errors. For the residual ML in the odd domains, the value of $d_3 = 3.08 \pm 0.07 \text{ \AA}$ is identical to the bulk value of 3.064 \AA and the buckling amplitude of $h_2 = 0.04 \pm 0.07 \text{ \AA}$ is slightly smaller than the bulk value of 0.2 \AA , which indicates that the residual ML has a bulk-Bi(110)-like structure. Therefore, we conclude that the even domains fully consist of BP-like BLs, and propose a new model for the odd domains, which consists of BP-like BLs and a bulk-Bi(110)-like ML located beneath the top BL.

The structural difference between the even and odd domains indicates subsurface structure transitions between them when a single ML is added during the growth, as depicted in Fig. 4(a). The new structure model for the odd domains would be preferable to the sandwich structure in regard to the structure transitions. The new model has only one different layer to the even structure, and all layers can have an in-phase in-plane lattice alignment with the neighboring even domains at the domain boundary, provided that the even and odd domains have the stacking structure shown in Figs. 1(b) and 1(d), respectively. This would lead to a relatively small interface energy at the domain boundary. In contrast, the sandwich structure requires all MLs but the top and bottom BLs to change and may cause a larger interface energy. We note that the new model has an out-of-phase surface lattice with respect to the even domain surface [see the top views of Figs. 1(b) and 1(d)]. This is inconsistent with a previous STM study that suggested the in-phase lattice alignment [28], but a recent STM study showed that the phase of surface lattice is not uniform due to numerous lattice displacements and inversions, indicating a difficulty in judging the lattice alignment [46]. Here, we assume that the film basically has the stacking structures of Figs. 1(b) and 1(d), considering the expected low interface energy.

Next, we discuss the growth behavior of the Bi(110) film. Figure 4(b) shows the change in coverage of each domain, derived from the layer coverages of Fig. S2(b) [42]. Initially, the 4-ML-thick BP-like domain is dominant, and then the odd domains appear with a smaller population than the even domains as shown in the odd/even population ratio of Fig. 4(d). We performed MC simulations to understand the growth behaviors. The simulations adopted the solid-on-solid model [48]. Details of the simulations are described in the Supplemental Material [42] (see, also, Refs. [31,49] therein). The parameters used in the simulations are shown in Fig. 5(a). A square grid of $(4.75 + 4.54)/2/\sqrt{2} = 3.3 \text{ \AA}$ was used for the location of Bi atoms, which provides the two orthogonal in-plane growth directions [see the top view in Fig. 5(a)].

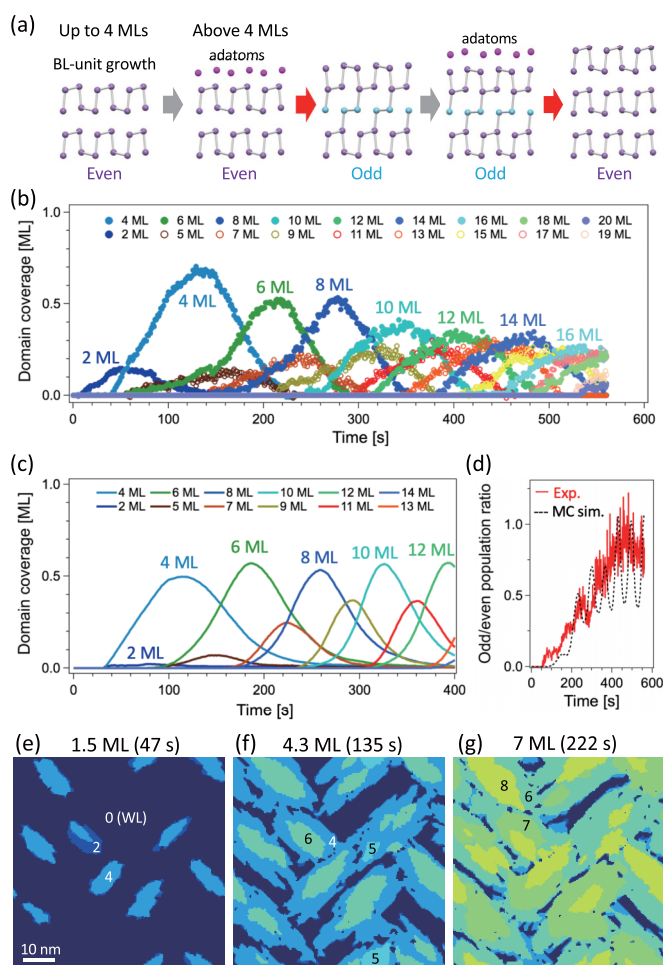


FIG. 4. (a) A model of the structure transitions during the growth of Bi(110) film. (b) Coverages of different height Bi(110) domains, obtained from the time-resolved CTR scattering data. Error bars are omitted for clarity. (c) Coverages of different height Bi(110) domains, obtained from the MC simulation. (d) Ratios of odd/even domain population derived from the experiments (solid line) and MC simulation (dashed line). (e)–(g) Domain structures of the Bi(110) film obtained by the MC simulation. The total coverage and deposition time are shown at the top. The thickness (the number of MLs) of each island is indicated.

The resulting coverage of each ML is shown in Fig. S3 [42], and the domain coverages and odd/even population ratio are shown in Figs. 4(c) and 4(d), respectively. They successfully reproduce the experimental features.

Snapshots of the simulated surface are shown in Figs. 4(e)–4(g). The following three features are consistent with the previous STM images [28,31,36,46]. (i) Initially 2-ML and 4-ML islands are nucleated [Fig. 4(e)], and then the even and odd domains grow on the 4-ML islands [Fig. 4(f)]. (ii) Most of the islands show an anisotropic shape with the preferential growth direction indicated in Fig. 5(a), due to the anisotropy of the in-plane bond energy ($E_C/E_{\text{HXY}} = 1.6/0.5$). (iii) Some of the even domains show BL-height islands, while the odd domains do not show them [e.g., Fig. 4(g)]; this is because the even domains allow the growth of BP-like BLs without the structure transitions while the odd domains do not allow

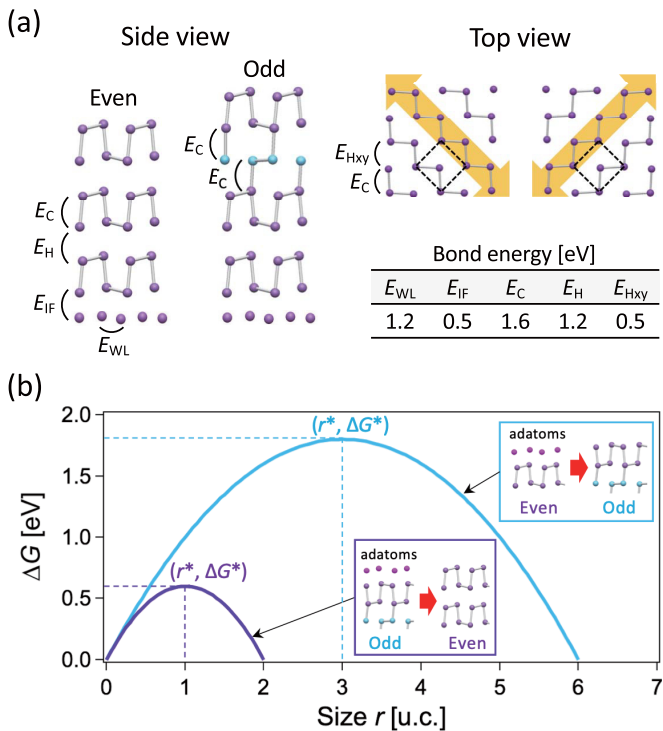


FIG. 5. (a) Parameters used in the MC simulations. Dashed rectangles indicate in-plane unit cells, and double-sided arrows indicate preferential growth directions. (b) Calculated free energy change ΔG with respect to the embryo size r for the even \rightarrow odd and odd \rightarrow even transitions. Dashed lines indicate the critical values of ΔG^* and r^* .

the direct growth (at least two transitions (odd \rightarrow even and even \rightarrow odd) are required).

In the MC simulations, the even \leftrightarrow odd structure transitions were assumed to occur with a probability proportional to $\exp[-\Delta G^*/(k_B T)]$ when the thickness exceeds four MLs and the size of embryo (even or odd domains with an adatom layer) exceeds a critical size of r^* , where ΔG^* is a change in the free energy of the system due to the structure transitions. The free energy change ΔG was defined as

$$\Delta G = n\Delta\mu - n_s\Delta\mu_s + n_b\sigma_b, \quad (1)$$

where the first term represents the energy change due to the creation (even \rightarrow odd) or destruction (odd \rightarrow even) of the bulk-Bi(110)-like ML (n is the number of atoms in the bulk-like ML and $\Delta\mu$ is the energy change per atom), the second term represents the change in surface energy (n_s is the number of surface atoms and $\Delta\mu_s$ is the energy per atom), and the third term represents the interface energy at the even/odd domain boundary induced by the transition (n_b is the number of atoms facing to the boundary and σ_b is the energy per

atom). Since the even and odd domains have the same surface structure and the domain boundary structure, we assumed that the second and third terms are common for both transitions.

The change in ΔG with respect to the embryo size r (in units of in-plane unit cell) is shown in Fig. 5(b). In the calculations, we used a simplified square-shaped system with $n = r^2 \times 2$ (the factor of 2 is due to the two atoms in the unit cell), $n_s = r^2 \times 2$, and $n_b = r \times 4 \times 2$. As shown in Fig. 5(b), the critical values of r^* and ΔG^* were estimated as 3 u.c. and 1.8 eV and 1 u.c. and 0.6 eV for the even \rightarrow odd and odd \rightarrow even transitions, respectively, provided that $\Delta\mu = 0.1$ eV and -0.1 eV for the even \rightarrow odd and odd \rightarrow even transitions, respectively, $\Delta\mu_s = 0.2$ eV, and $\sigma_b = 0.15$ eV. The values of $\Delta\mu$ and $\Delta\mu_s$ would be reasonable according to the theoretical studies [32,37]. The critical values were used in the MC simulation to successfully reproduce the experimental results. When $\Delta\mu = 0$, a conventional layer-by-layer growth appeared and the preferential even domain formation was not reproduced (see Figs. S4(a) and S4(b) [42]). When the interface energy σ_b increased to 0.3 eV, the critical values for the even \rightarrow odd transition become $\Delta G^* = 7.2$ eV and $r^* = 6$ u.c. and the transition hardly occurred. Therefore, we conclude that the smaller free energy of the even domains leads to the preferential even domain formation and that the relatively small interface energy due to the structural similarity between the even and odd domains allows the frequent structure transitions during the growth.

III. SUMMARY

In summary, real-time CTR scattering measurements revealed the structure and growth behaviors of Bi(110) films grown on Si(111)- 7×7 . The film shows the BL-unit growth up to four MLs and a quasi-ML-by-ML growth above four MLs with a preference of the even domains. The even domains fully consist of the BP-like BLs and the odd domains have an additional bulk-Bi(110)-like ML located beneath the top BL. The preferential formation of the even domains is due to a smaller free energy than the odd domains and a relatively small interface energy at the even/odd domain boundary allows the frequent even \leftrightarrow odd structure transitions during the growth. The structure and growth behaviors revealed by this study provide new insights into research of electronic and topological properties of the Bi(110) films. The results also highlight the ability of the real-time CTR scattering method for the study of irreversible phenomena at surfaces and interfaces such as thin film growth.

ACKNOWLEDGMENT

All the synchrotron radiation experiments were done at the Photon Factory, KEK (PF-PAC No.2018G661 and No. 2020G505).

[1] Y. Xu, Z. Shi, X. Shi, K. Zhang, and H. Zhang, Recent progress in black phosphorus and black-phosphorus-analogue materials: Properties, synthesis and applications, *Nanoscale* **11**, 14491 (2019).

[2] S. Zhang, S. Guo, Z. Chen, Y. Wang, H. Gao, J. Gómez-Herrero, P. Ares, F. Zamora, Z. Zhu, and H. Zeng, Recent progress in 2D group-VA semiconductors: From theory to experiment, *Chem. Soc. Rev.* **47**, 982 (2018).

- [3] Z. Wu and J. Hao, Electrical transport properties in group-V elemental ultrathin 2D layers, *npj 2D Mater. Appl.* **4**, 4 (2020).
- [4] Z. Shi, X. Ren, H. Qiao, R. Cao, Y. Zhang, X. Qi, and H. Zhang, Recent insights into the robustness of two-dimensional black phosphorus in optoelectronic applications, *J. Photochem. Photobiol. C* **43**, 100354 (2020).
- [5] M. Qiu, Z. T. Sun, D. K. Sang, X. G. Han, H. Zhang, and C. M. Niu, Current progress in black phosphorus materials and their applications in electrochemical energy storage, *Nanoscale* **9**, 13384 (2017).
- [6] J. Geng, S. Chen, and X. Chen, State-of-the-art applications of 2D nanomaterials in energy storage, in *Adapting 2D Nanomaterials for Advanced Applications* (American Chemical Society, Washington, D.C., 2020), Chap. 11, pp. 253–293.
- [7] X. Yu, W. Liang, C. Xing, K. Chen, J. Chen, W. Huang, N. Xie, M. Qiu, X. Yan, Z. Xie, and H. Zhang, Emerging 2D pnictogens for catalytic applications: Status and challenges, *J. Mater. Chem. A* **8**, 12887 (2020).
- [8] L. Li, Y. Yu, G. J. Ye, Q. Ge, X. Ou, H. Wu, D. Feng, X. H. Chen, and Y. Zhang, Black phosphorus field-effect transistors, *Nature Nanotechnol.* **9**, 372 (2014).
- [9] T. Low, A. S. Rodin, A. Carvalho, Y. Jiang, H. Wang, F. Xia, and A. H. Castro Neto, Tunable optical properties of multi-layer black phosphorus thin films, *Phys. Rev. B* **90**, 075434 (2014).
- [10] L.-Q. Sun, M.-J. Li, K. Sun, S.-H. Yu, R.-S. Wang, and H.-M. Xie, Electrochemical activity of black phosphorus as an anode material for lithium-ion batteries, *J. Phys. Chem. C* **116**, 14772 (2012).
- [11] Q. Jiang, L. Xu, N. Chen, H. Zhang, L. Dai, and S. Wang, Facile synthesis of black phosphorus: An efficient electrocatalyst for the oxygen evolving reaction, *Angew. Chem. Int. Ed.* **55**, 13849 (2016).
- [12] Y. Lu, W. Xu, M. Zeng, G. Yao, L. Shen, M. Yang, Z. Luo, F. Pan, K. Wu, T. Das, P. He, J. Jiang, J. Martin, Y. P. Feng, H. Lin, and X.-s. Wang, Topological properties determined by atomic buckling in self-assembled ultrathin Bi(110), *Nano Lett.* **15**, 80 (2015).
- [13] S.-s. Li, W.-x. Ji, P. Li, S.-j. Hu, L. Cai, C.-w. Zhang, and S.-s. Yan, Tunability of the quantum spin hall effect in Bi(110) films: Effects of electric field and strain engineering, *ACS Appl. Mater. Interfaces* **9**, 21515 (2017).
- [14] P. J. Kowalczyk, S. A. Brown, T. Maerkl, Q. Lu, C.-K. Chiu, Y. Liu, S. A. Yang, X. Wang, I. Zasada, F. Genuzio, T. O. Menteş, A. Locatelli, T.-C. Chiang, and G. Bian, Realization of symmetry-enforced two-dimensional dirac fermions in nonsymmorphic α -bismuthene, *ACS Nano* **14**, 1888 (2020).
- [15] T. Märkl, P. J. Kowalczyk, M. L. Ster, I. V. Mahajan, H. Pirie, Z. Ahmed, G. Bian, X. Wang, T.-C. Chiang, and S. A. Brown, Engineering multiple topological phases in nanoscale van der waals heterostructures: Realisation of α -antimonene, *2D Mater.* **5**, 011002 (2017).
- [16] K.-H. Jin, H. Huang, Z. Wang, and F. Liu, A 2D nonsymmorphic dirac semimetal in a chemically modified group-va monolayer with a black phosphorene structure, *Nanoscale* **11**, 7256 (2019).
- [17] Y. Bai, L. Cai, N. Mao, R. Li, Y. Dai, B. Huang, and C. Niu, Doubled quantum spin hall effect with high-spin chern number in α -antimonene and α -bismuthene, *Phys. Rev. B* **105**, 195142 (2022).
- [18] T. Nagao, J. T. Sadowski, M. Saito, S. Yaginuma, Y. Fujikawa, T. Kogure, T. Ohno, Y. Hasegawa, S. Hasegawa, and T. Sakurai, Nanofilm Allotrope and Phase Transformation of Ultrathin Bi Film on Si(111)- 7×7 , *Phys. Rev. Lett.* **93**, 105501 (2004).
- [19] S. Hatta, Y. Ohtsubo, S. Miyamoto, H. Okuyama, and T. Aruga, Epitaxial growth of Bi thin films on Ge(111), *Appl. Surf. Sci.* **256**, 1252 (2009).
- [20] J. T. Sun, H. Huang, S. L. Wong, H. J. Gao, Y. P. Feng, and A. T. S. Wee, Energy-Gap Opening in a Bi(110) Nanoribbon Induced by Edge Reconstruction, *Phys. Rev. Lett.* **109**, 246804 (2012).
- [21] P. J. Kowalczyk, D. Belic, O. Mahapatra, S. A. Brown, E. S. Kadantsev, T. K. Woo, B. Ingham, and W. Kozłowski, Anisotropic oxidation of bismuth nanostructures: Evidence for a thin film allotrope of bismuth, *Appl. Phys. Lett.* **100**, 151904 (2012).
- [22] P. J. Kowalczyk, O. Mahapatra, S. A. Brown, G. Bian, X. Wang, and T.-C. Chiang, Electronic size effects in three-dimensional nanostructures, *Nano Lett.* **13**, 43 (2013).
- [23] P. J. Kowalczyk, O. Mahapatra, M. Le Ster, S. A. Brown, G. Bian, X. Wang, and T.-C. Chiang, Single atomic layer allotrope of bismuth with rectangular symmetry, *Phys. Rev. B* **96**, 205434 (2017).
- [24] L. Peng, J. Qiao, J.-J. Xian, Y. Pan, W. Ji, W. Zhang, and Y.-S. Fu, Unusual electronic states and superconducting proximity effect of bi films modulated by a NbSe₂ substrate, *ACS Nano* **13**, 1885 (2019).
- [25] E. Gaufrés, F. Fossard, V. Gosselin, L. Sponza, F. Ducastelle, Z. Li, S. G. Louie, R. Martel, M. Côté, and A. Loiseau, Momentum-resolved dielectric response of free-standing mono-, bi-, and trilayer black phosphorus, *Nano Lett.* **19**, 8303 (2019).
- [26] L. Zhou, J. Chen, X. Chen, B. Xi, Y. Qiu, J. Zhang, L. Wang, R. Zhang, B. Ye, P. Chen, X. Zhang, G. Guo, D. Yu, J.-W. Mei, F. Ye, G. Wang, and H. He, Topological hall effect in traditional ferromagnet embedded with black-phosphorus-like bismuth nanosheets, *ACS Appl. Mater. Interfaces* **12**, 25135 (2020).
- [27] I. Kokubo, Y. Yoshiike, K. Nakatsuji, and H. Hirayama, Ultrathin Bi(110) films on Si(111) $\sqrt{3} \times \sqrt{3}$ -B substrates, *Phys. Rev. B* **91**, 075429 (2015).
- [28] K. Nagase, I. Kokubo, S. Yamazaki, K. Nakatsuji, and H. Hirayama, Structure and growth of Bi(110) islands on Si(111) $\sqrt{3} \times \sqrt{3}$ -B substrates, *Phys. Rev. B* **97**, 195418 (2018).
- [29] S. Ju, M. Wu, H. Yang, N. Wang, Y. Zhang, P. Wu, P. Wang, B. Zhang, K. Mu, Y. Li, D. Guan, D. Qian, F. Lu, D. Liu, W.-H. Wang, X. Chen, and Z. Sun, Band structures of ultrathin Bi(110) films on black phosphorus substrates using angle-resolved photoemission spectroscopy, *Chin. Phys. Lett.* **35**, 077102 (2018).
- [30] X. Dong, Y. Li, J. Li, X. Peng, L. Qiao, D. Chen, H. Yang, X. Xiong, Q. Wang, X. Li, J. Duan, J. Han, and W. Xiao, Epitaxial growth and structural properties of Bi(110) thin films on TiSe₂ substrates, *J. Phys. Chem. C* **123**, 13637 (2019).
- [31] R. Ushioda, M. Shimura, K. Nakatsuji, and H. Hirayama, Growth-rate dependence of the structural transition of bismuth islands on Si(111) substrates, *Phys. Rev. Mater.* **6**, 043403 (2022).
- [32] E. Aktürk, O. U. Aktürk, and S. Ciraci, Single and bilayer bismuthene: Stability at high temperature and mechanical and electronic properties, *Phys. Rev. B* **94**, 014115 (2016).

- [33] J. Dai and X. C. Zeng, Bilayer phosphorene: Effect of stacking order on bandgap and its potential applications in thin-film solar cells, *J. Phys. Chem. Lett.* **5**, 1289 (2014).
- [34] H. Shu, Y. Li, X. Niu, and J. Wang, The stacking dependent electronic structure and optical properties of bilayer black phosphorus, *Phys. Chem. Chem. Phys.* **18**, 6085 (2016).
- [35] G. Moynihan, S. Sanvito, and D. D. O'Regan, Strain-induced weyl and dirac states and direct-indirect gap transitions in group-V materials, *2D Mater.* **4**, 045018 (2017).
- [36] J. Wang, X. Sun, H. Du, C. Ma, and B. Wang, Electronic and topological properties of Bi(110) ultrathin films grown on a cu(111) substrate, *Phys. Rev. B* **105**, 115407 (2022).
- [37] G. Bian, X. Wang, T. Miller, T.-C. Chiang, P. J. Kowalczyk, O. Mahapatra, and S. A. Brown, First-principles and spectroscopic studies of Bi(110) films: Thickness-dependent dirac modes and property oscillations, *Phys. Rev. B* **90**, 195409 (2014).
- [38] T. Matsushita, T. Takahashi, T. Shirasawa, E. Arakawa, H. Toyokawa, and H. Tajiri, Quick measurement of crystal truncation rod profiles in simultaneous multi-wavelength dispersive mode, *J. Appl. Phys.* **110**, 102209 (2011).
- [39] T. Shirasawa, T. Masuda, W. Voegeli, E. Arakawa, C. Kamezawa, T. Takahashi, K. Uosaki, and T. Matsushita, Fast structure determination of electrode surfaces for investigating electrochemical dynamics using wavelength-dispersive x-ray crystal truncation rod measurements, *J. Phys. Chem. C* **121**, 24726 (2017).
- [40] W. Voegeli, T. Matsushita, E. Arakawa, T. Shirasawa, T. Takahashi, and Y. F. Yano, A method for measuring the specular x-ray reflectivity with millisecond time resolution, *J. Phys. Conf. Ser.* **425**, 092003 (2013).
- [41] T. Shirasawa, W. Voegeli, E. Arakawa, T. Takahashi, and T. Matsushita, Structural change of the rutile-TiO₂(110) surface during the photoinduced wettability conversion, *J. Phys. Chem. C* **120**, 29107 (2016).
- [42] See Supplemental Material at <http://link.aps.org/supplemental/10.1103/PhysRevMaterials.7.033404> for the details of real-time CTR experiments, structure analysis, and MC simulations; the detector images and measured and calculated CTR profiles.
- [43] K. Nagase, R. Ushioda, K. Nakatsuji, T. Shirasawa, and H. Hirayama, Growth of extremely flat Bi(110) films on a Si(111) $\sqrt{3} \times \sqrt{3}$ -B substrate, *Appl. Phys. Express* **13**, 085506 (2020).
- [44] See Supplemental Material at <http://link.aps.org/supplemental/10.1103/PhysRevMaterials.7.033404> for the detector images and measured and calculated CTR profiles.
- [45] T. Shirasawa, M. Ohyama, W. Voegeli, and T. Takahashi, Interface of a Bi(001) film on Si(111)-7 \times 7 imaged by surface x-ray diffraction, *Phys. Rev. B* **84**, 075411 (2011).
- [46] Y. Lyu, S. Daneshmandi, S. Huyan, and C. Chu, Flexible atomic buckling and homogeneous edge states in few-layer Bi(110) films, *Nano Res.* **15**, 2374 (2022).
- [47] D. Guo, P. Guo, S. Tan, M. Feng, L. Cao, Z.-X. Liu, K. Liu, Z.-Y. Lu, and W. Ji, Two-dimensional dirac-line semimetals resistant to strong spinorbit coupling, *Sci. Bull.* **67**, 1954 (2022).
- [48] C. I. Fornari, G. Fornari, P. H. de O. Rappl, E. Abramof, and J. dos S. Travelho, in *Epitaxy*, edited by M. Zhong (IntechOpen, 2018), Chap. 5, pp. 113–129.
- [49] T. Irisawa, Y. Arima, and T. Kuroda, Periodic changes in the structure of a surface growing under mbe conditions, *J. Cryst. Growth* **99**, 491 (1990).